

PREFACE FIGURES

22/06/19

chazla que es grande
toda la página

0.1. VIEWS OF THE NUCLEUS

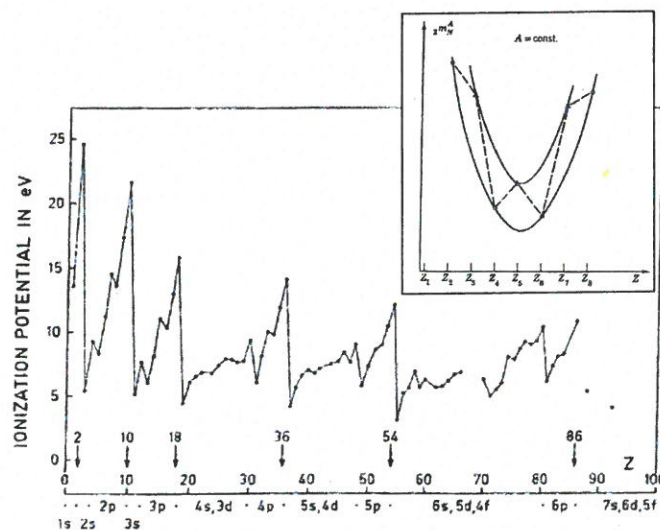


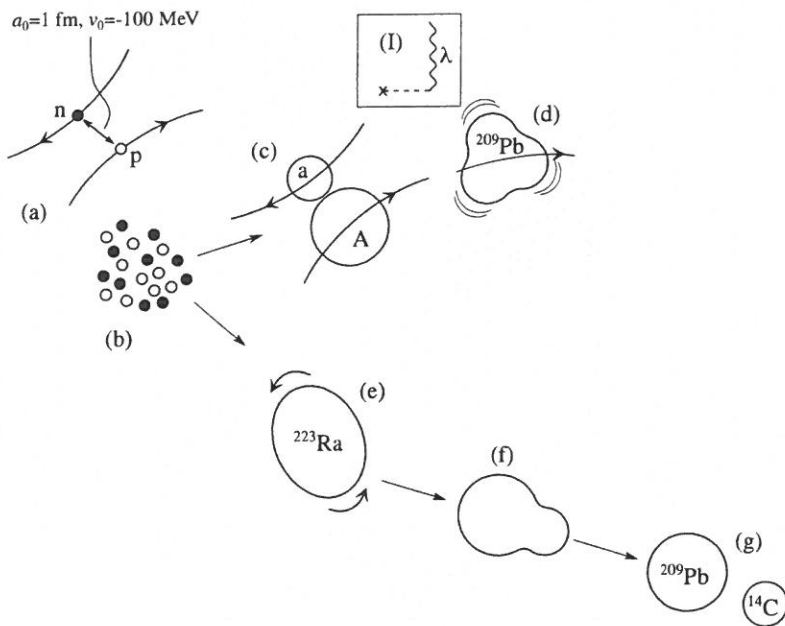
Figura muy grande
no se ve
7 La caption
es corta

✓ Figure 0.1.1: The values of the atomic ionization potentials. The dots under the abscissa indicate closed shells, corresponding to electron numbers: 2(He), 10(Ne), 18(Ar), 36(Kr), 54(Xe), and 86(Ra). After Bohr and Mottelson (1969). In the inset, masses of nuclei with even A are shown (after Mayer and Jensen (1955)).

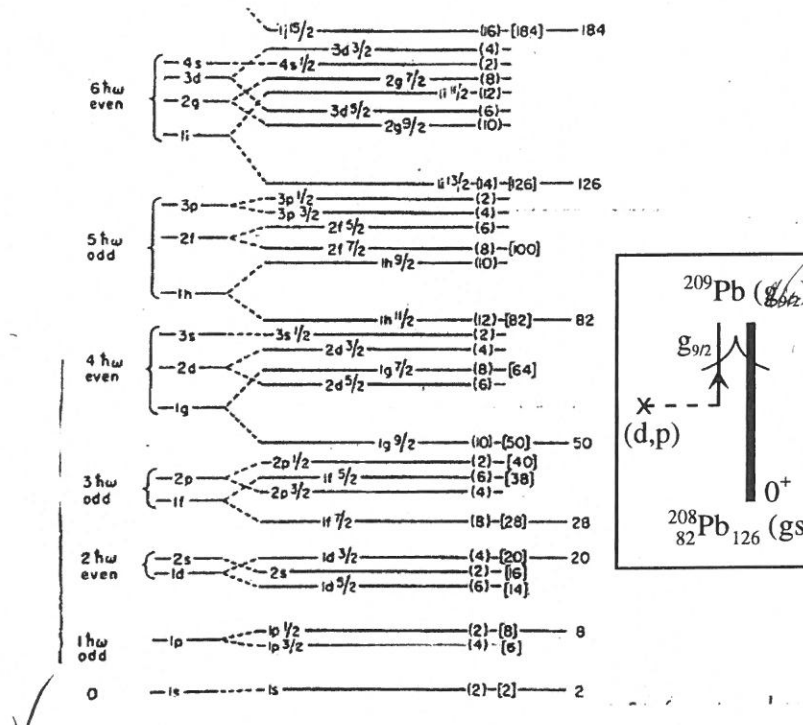
the proper interaction leading to realistic Hartree-Fock mean field and collective RPA particle-hole and pairing vibrational modes. As one possible return of such input, nuclear field theory will eventually be able to provide shell model practitioners, friendly and accurate microscopic collective modes of excitation input.

The possible outcome of such collaboration and interplay could be that of being able to coin into few physical concepts the elements needed to accurately describe the atomic nucleus. In other words, carry out calculations which are largely independent of the basis chosen. That is truly predictive theories of structure and reactions, in which the physical content is simple to apprehend and visualize.

Figura
mas
grande



✓ Figure 0.1.2: Emergent properties (collective nuclear models) (a) Nucleon-Nucleon (NN) interaction in a scattering experiment; (b) assembly of a swarm of nucleons condensing into drops of nuclear matter, examples shown in (c) and (e); (c) anelastic heavy ion reaction $a + A \rightarrow a + A^*$ setting the nucleus A into an octupole surface oscillations (d); in inset (I) the time-dependent nuclear plus Coulomb fields associated with the reaction (c) is represented by a cross followed by a dashed line, while the wavy line labeled λ describes the propagation of the surface vibration shown in (d), time running upwards; (e) another possible outcome of nucleon condensation: the (weakly) quadrupole deformed nucleus ^{223}Ra which can rotate as a whole with moment of inertia smaller than the rigid moment of inertia, but much larger than the irrotational one; (f) the surface of a quantal drop fluctuates (zero point fluctuations), with the variety of multipolarities with which the system reacts to time-dependent Coulomb/nuclear external fields (quadrupole ($\lambda = 2$), octupole ($\lambda = 3$), etc.), eventually producing a neck-in (saddle conformation) and the exotic decay $^{223}\text{Ra} \rightarrow ^{209}\text{Pb} + ^{14}\text{C}$ as experimentally observed (g).

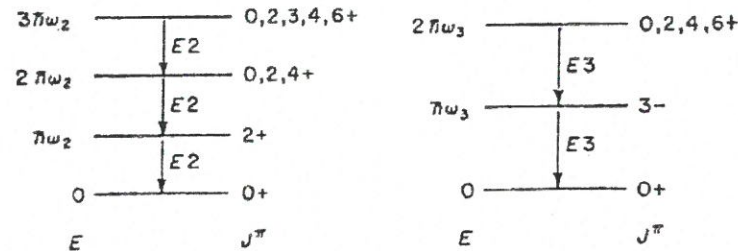


✓ Figure 0.1.3: To the left (first column), the sequence of levels of the harmonic oscillator potential labeled with the total oscillator quantum number and parity $\pi = (-1)^N$. The next column shows the splitting of major shell degeneracies obtained using a more realistic potential (Woods-Saxon), the quantum number being the number of radial nodes of the associated single-particle wave functions. The levels shown at the center result when a spin-orbit term is considered the quantum numbers nlj characterizing the states of degeneracy $(2j + 1)$ ($j = |l \pm 1/2|$) (After Mayer (1963)). In the inset, a schematic graphical representation of the reaction $^{208}_{82}\text{Pb}_{126}(d, p)^{209}_{82}\text{Pb}_{126}(\text{gs})$ is shown. A cross followed by a horizontal dashed line represents here the (d, p) field, while a single arrowed line describes the odd nucleon moving in the $g_{9/2}$ orbital above $N = 126$ shell closure drawn as a bold line labeled 0^+ .

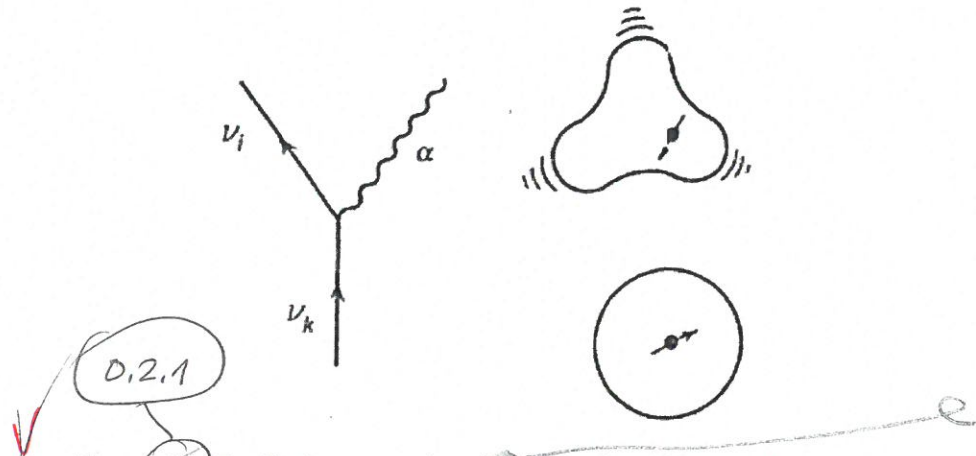
(and belonging to the $N = 8$ major shell)

$\ell \pm 1/2$
no absolute value

(after Bohr and Mottebo (1969))



✓ Figure 0.1.4: Schematic representation of Harmonic quadrupole and octupole liquid drop collective surface vibrational modes.



✓ Figure 0.1.5: Graphical representation of the process by which a fermion, bouncing inelastically off the surface, sets it into vibration. Particles are represented by an arrowed line, while the vibration is shown by a wavy line. The black dot represents a nucleon moving in a spherical mean field of which it excites an octupole vibration after bouncing inelastically off the surface.

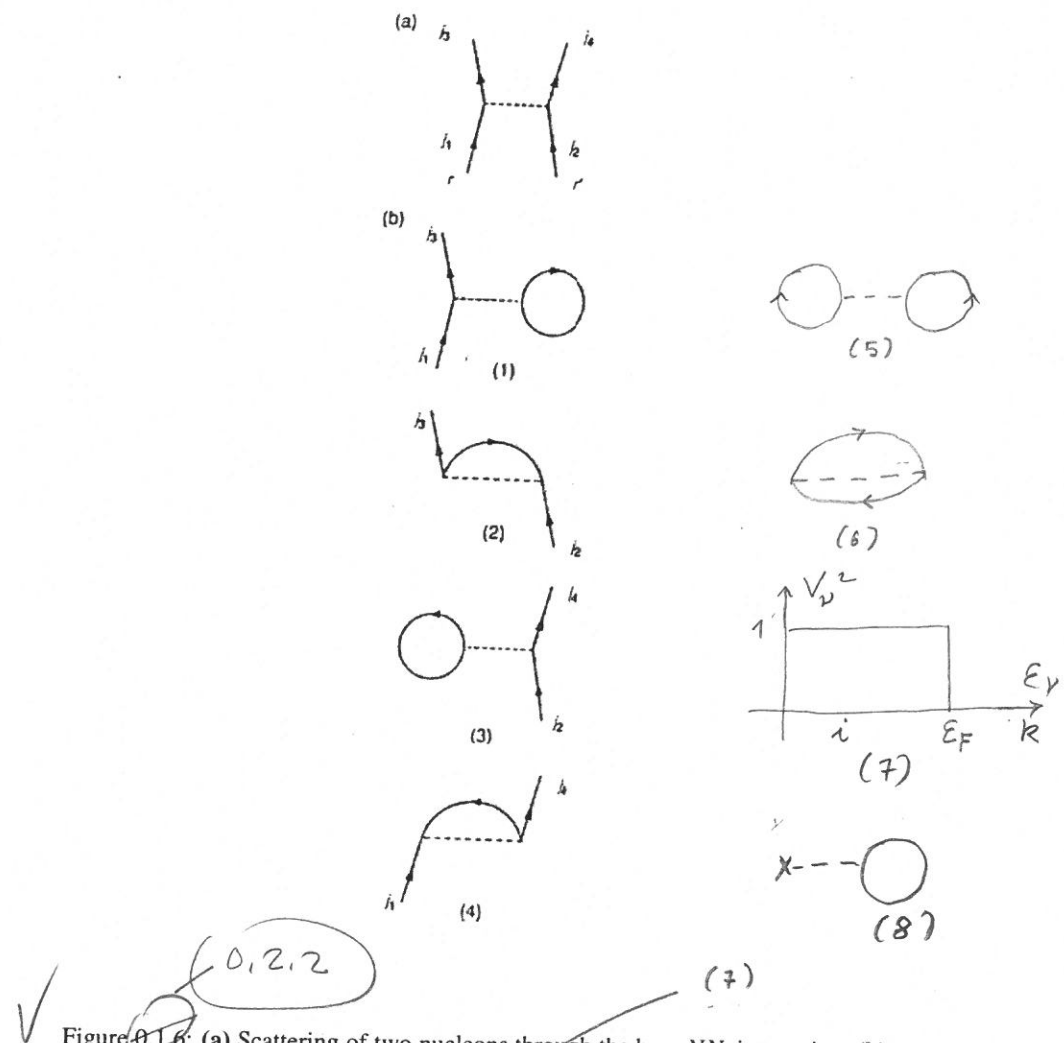
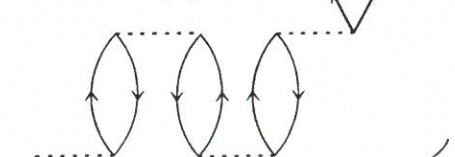


Figure 0.1.6: (a) Scattering of two nucleons through the bare NN -interaction; (b) (1) and (3): Contributions to the (direct) Hartree potential; (2) and (4): contributions to the (exchange) Fock potential. In (5) and (6) the ground state correlations associated with the Hartree and the Fock-terms are displayed. States $|i\rangle$ ($E_i \leq E_F$) are occupied with probability $V_i^2 = 1$, States $|k\rangle$ ($E_k > E_F$) are empty $V_k^2 = 1 - V_i^2 = 0$. (8) Nuclear density, the density operator being represented by a cross followed by a dashed horizontal line. (After Brink and Broglie (2005))

20.8.19
Hartree-Fock

$$(a) \quad \alpha = \sum_{\nu_k \nu_i} \nu_k \nu_i + \quad (b) \quad \nu_k \quad \nu_i + \quad (c) \quad \nu_k \quad \nu_i$$

(A)



The amplitudes

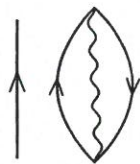
; leading to the amplitudes $X_{hi}^{\alpha} = \frac{1\alpha \langle \tilde{v} | F | k \rangle}{(\epsilon_k - \epsilon_i) - \hbar\omega}$
where $1\alpha = k \sqrt{\frac{\hbar\omega}{2\epsilon_0}}$

$(1/2)\hbar\omega$

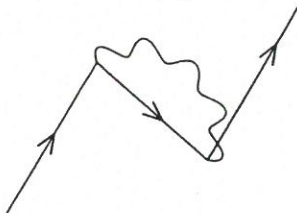
✓ Figure 0.1.7: (A) typical Feynman diagram diagonalizing the NN -interaction $v(|r-r'|)$ (horizontal dashed line) in a particle-hole basis provided by the Hartree-Fock solution of v , in the harmonic approximation (RPA). Bubbles going forward in time (inset (b)) are associated with configuration mixing of particle-hole states. Bubbles going backwards in time (inset (c)) are associated with zero point motion (fluctuations ZPF) of the ground state (term $1/2\hbar\omega$ for each degree of freedom in Eq. 0.1.11). The self consistent solution of A is represented by a wavy line (inset (a)), that is a collective mode which can be viewed as a correlated particle hole excitation.

(D, 2, 3)

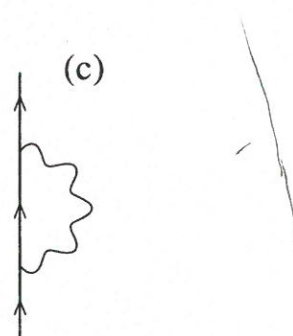
(a)



(b)



(c)



✓ Figure 0.1.8: (a) a nucleon (single arrowed line) moving in presence of the zero point fluctuation of the nuclear ground state associated with a collective surface vibration; (b) Pauli principle leads to a dressing event of the nucleon; (c) time ordering gives rise to the second possible lowest order clothing process (time assumed to run upwards).

0, 2, 4

, eigenstates of the dispersion relation $\sum_{ki} \frac{2(\epsilon_k - \epsilon_i) |\langle \tilde{v} | F | k \rangle|^2}{(\epsilon_k - \epsilon_i)^2 - (\hbar\omega\alpha)^2} = 1/k$

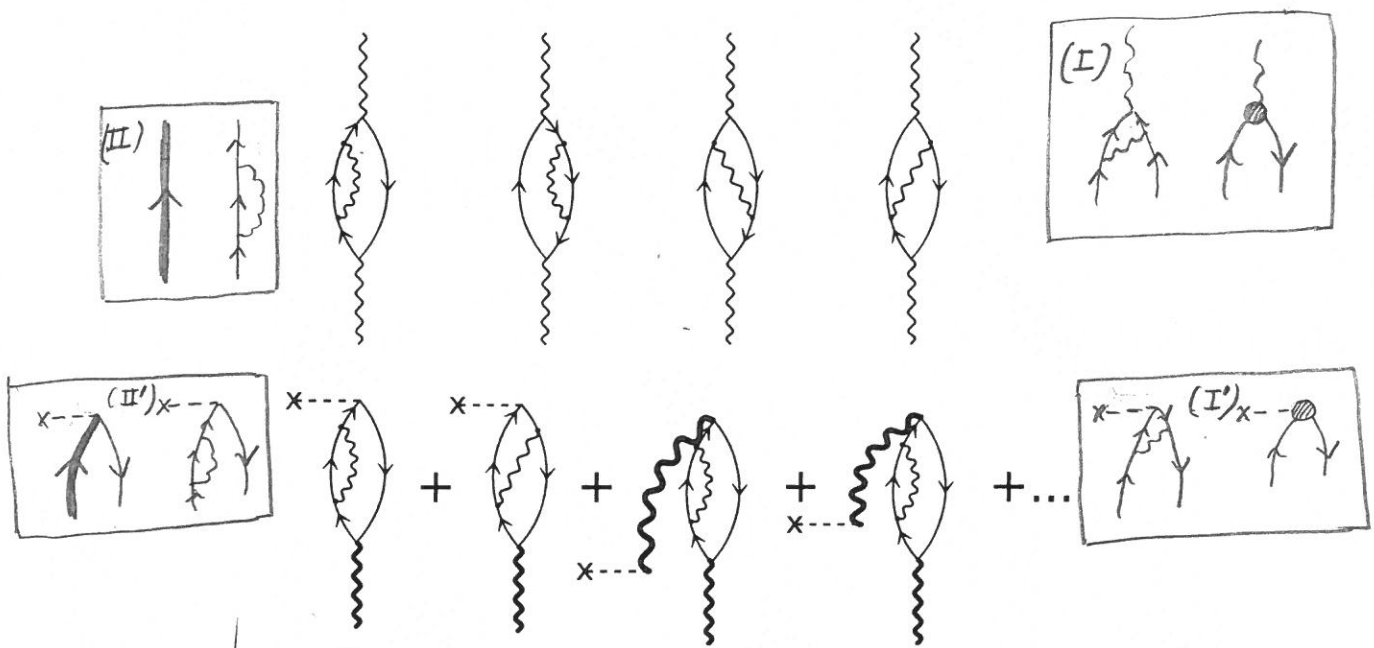


Figure 0.1.9: (Upper part) Examples of renormalization processes dressing a surface collective vibrational state. (Lower part) Intervening with an external electromagnetic field ($E\lambda$: cross followed by dashed horizontal line; bold wavy lines, renormalized vibration of multipolarity λ) the $B(E\lambda)$ transition strength can be measured.

In insets (I) and (I'), the hatched circle stands for the renormalised PVC strength and the effective charge respectively.

In (II) and (II') the bold face arrowed curve represent the motion of a nucleon of effective mass m^* in a potential $(m/m^*)U(r)$, $U(r)$ being the potential describing the motion of nucleon of bare mass m described by normal arrowed lines (see e.g. Brueh and Broglia (2005) App. B).

$$(a) \quad x_{--} = \sum_k x_{--}^{(k)} + \sum_i x_{--}^{(i)}$$

Fig. 0.1.41

(0.3.1)

$$(c) \quad x_{--}^{(i)}$$

(represented by a double arrowed line)

Graphical representation of the RPA dispersion relation describing the pair addition pairing vibrational mode, making use of the unitarity transformation (0.1.34); a cross followed by a dashed horizontal line stands for: (a) the collective operator Γ_{α}^+ ; (b) the operator Γ_k^+ creating a pair of nucleons moving in time reversal states (k, \bar{k}); above the Fermi energy ($E_k > E_F$); (c) The operator Γ_i^+ filling a pair of time reversal holes ($E_i < E_F$)

20/6/19

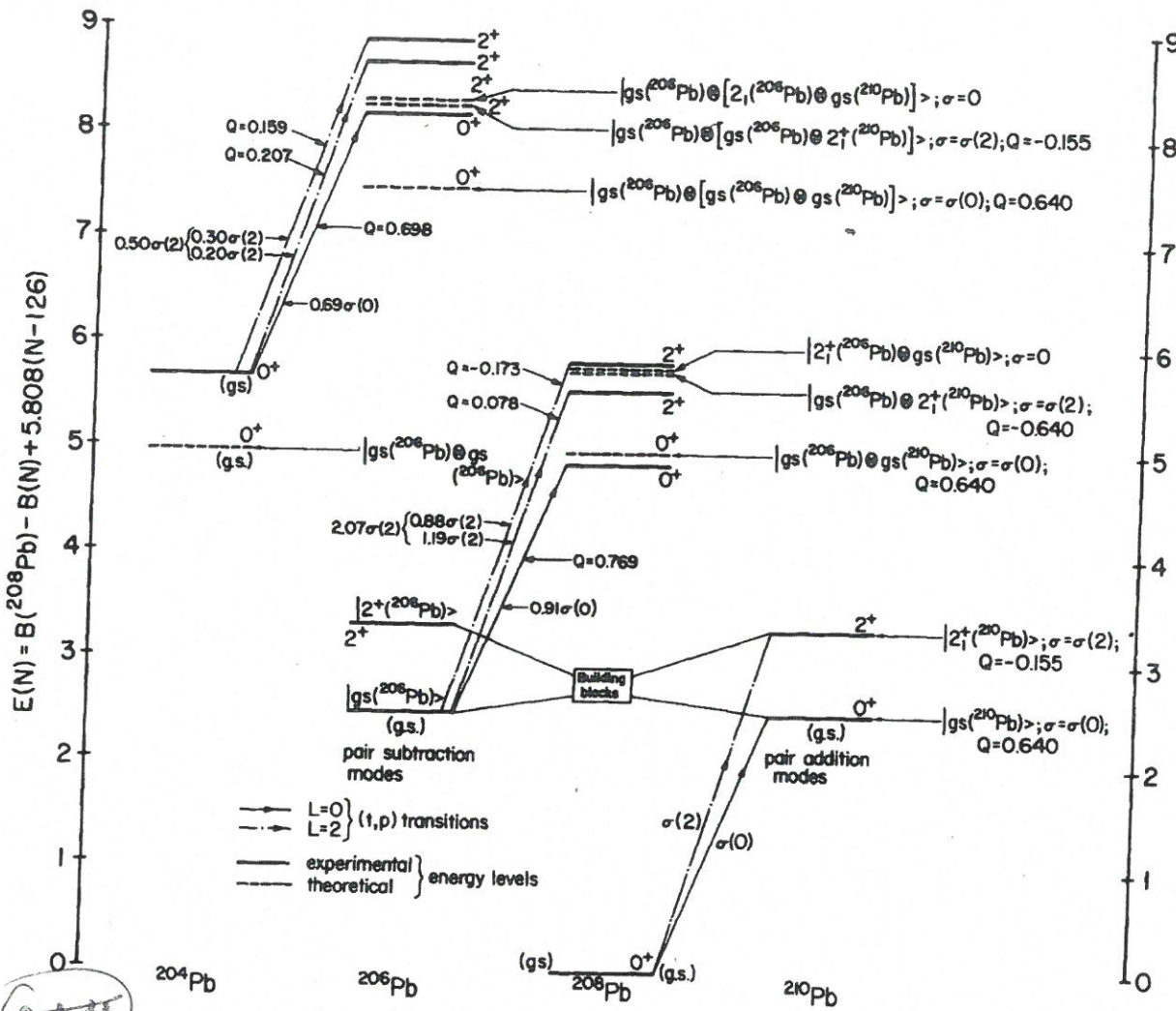


Fig. 1. Theoretical predictions of the pairing vibrational model for the $J^\pi = 0^+$ and 2^+ excited states of ^{208}Pb and ^{206}Pb expected to display the same Q -value, angular distribution and intensities in the $^{206},^{204}\text{Pb}$ (t, p) reactions as the ground state and first excited 2^+ state of ^{210}Pb in the ^{208}Pb (t, p) ^{210}Pb reaction.

These levels are depicted as dotted lines and their structure in terms of the pair addition and pair subtraction phonons (building blocks) are explicitly given.

The corresponding cross section and Q -values expected for each transition are also quoted for each state. The experimental energies (solid lines) and (t, p) cross sections are also given. In this case, the levels are joined by a continuous line ($L = 0$ transitions) or by a dotted line ($L = 2$ transitions) and the corresponding intensities in terms of the cross sections $\sigma(0) = \sigma(^{208}\text{Pb} (t, p) ^{210}\text{Pb} (\text{gs}))$ and $\sigma(2) = \sigma(^{208}\text{Pb} (t, p) ^{210}\text{Pb} (2^+))$ are given. Also quoted are the observed Q -values.

The experimental energy of the different ground states is given relative to the ^{208}Pb ground state and corrected by a linear function of the number of neutrons outside (or missing from) the $N = 126$ closed shell such that $E(^{206}\text{Pb} (\text{gs})) = E(^{210}\text{Pb} (\text{gs}))$. The corresponding expression [6] is $E_{\text{exp}}(N, Z = 82) = B(^{208}\text{Pb}) - B(N, Z = 82) + 5.808(N-126)$, where $B(N, Z)$ is the binding energy of the nucleus $A = N + Z$. Note that $\hbar\omega(0) = E_{\text{theor}}(^{206}\text{Pb} (\text{gs})) = E_{\text{theor}}(^{210}\text{Pb} (\text{gs})) = E_{\text{exp}}(^{206}\text{Pb} (\text{gs})) = E_{\text{exp}}(^{210}\text{Pb} (\text{gs})) = 2.493$ MeV, that $E_{\text{theor}}(^{206}\text{Pb} (2^+)) = E_{\text{exp}}(^{206}\text{Pb} (2^+)) = 3.294$ MeV and $E_{\text{theor}}(^{210}\text{Pb} (2^+)) = E_{\text{exp}}(^{210}\text{Pb} (2^+)) = 3.288$ MeV. The theoretical energy of any other state, for example of the 2^+ state $|gs(^{206}\text{Pb}) \otimes 2(^{210}\text{Pb}); 2^+\rangle$ of ^{206}Pb is equal to $2.493 + 3.294 + 2.493 = 8.280$ MeV (as measured from $^{208}\text{Pb} (\text{gs})$).

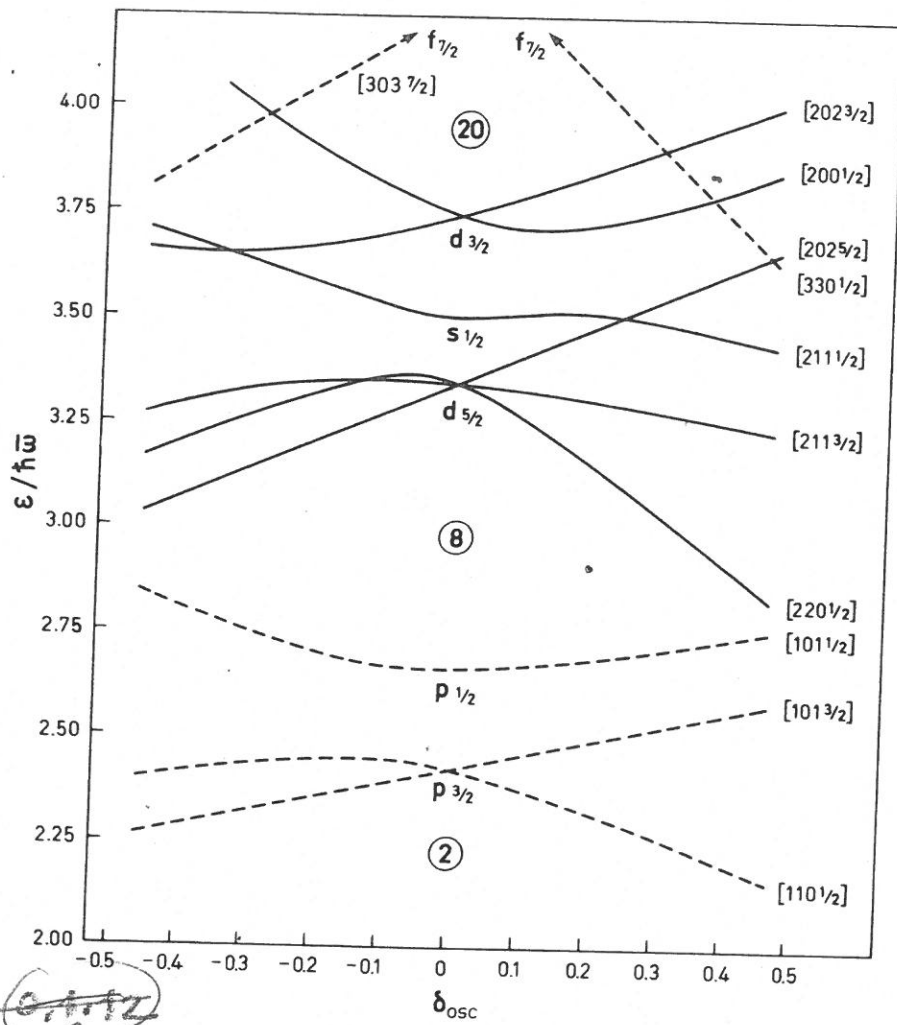
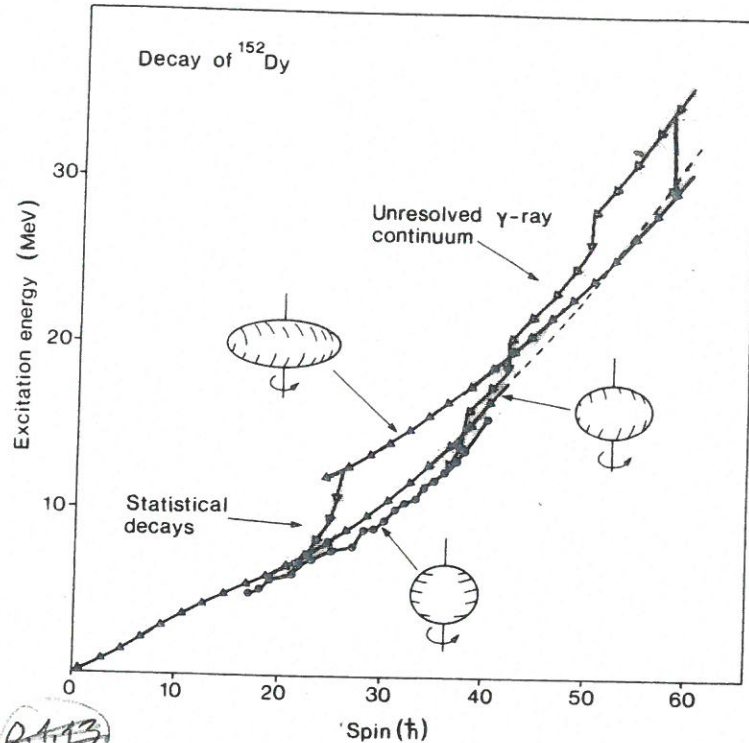


Figure 5-1 Spectrum of single-particle orbits in spheroidal potential (N and $Z < 20$). The spectrum is taken from B. R. Mottelson and S. G. Nilsson, *Mat. Fys. Skr. Dan. Vid. Selsk.* 1, no. 8 (1959). The orbits are labeled by the asymptotic quantum numbers $[Nn_3\Lambda\Omega]$ referring to large prolate deformations. Levels with even and odd parity are drawn with solid and dashed lines, respectively.

(after Bohr and Mottelson (1975))

✓ *(Signature)*
0,4,1



✓ *D.4.13*
 Figure 8 A schematic of the proposed γ -ray decay paths from a high-spin entry point in ^{152}Dy . The major initial decay flow occurs mainly via E2 transitions in the unresolved γ -ray continuum and reaches the oblate yrast structures between $30\hbar$ and $40\hbar$. A small 1% branch feeds the superdeformed band, which is assumed to become yrast at a spin of $50-55\hbar$. The deexcitation of the superdeformed band around $26\hbar$ occurs when the band is 3-5 MeV above yrast, and a statistical type of decay flow takes it into the oblate states between $19\hbar$ and $25\hbar$. The diagram also shows the low deformation prolate band (After Nolan and Twin (1988)).

P. J. Nolan and P. Twin, Superdeformed charge at high angular momentum, Ann. Rev. Nucl. and Particle Science, 38, 533 (1988)

D.4.2

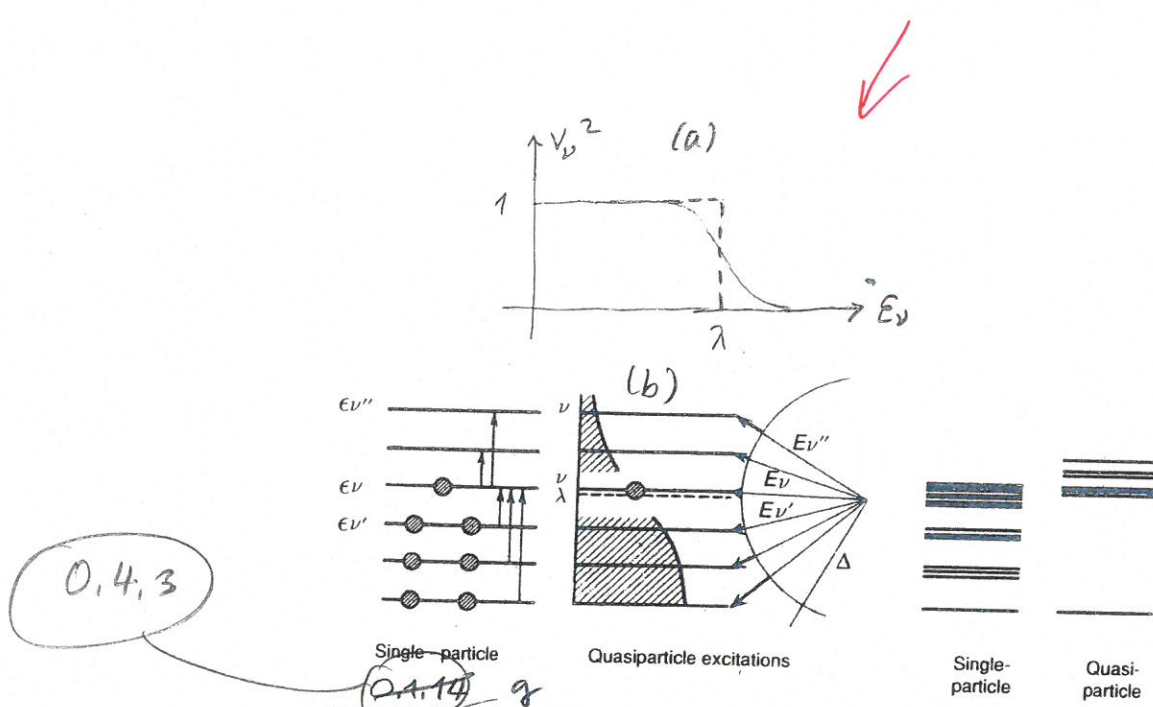
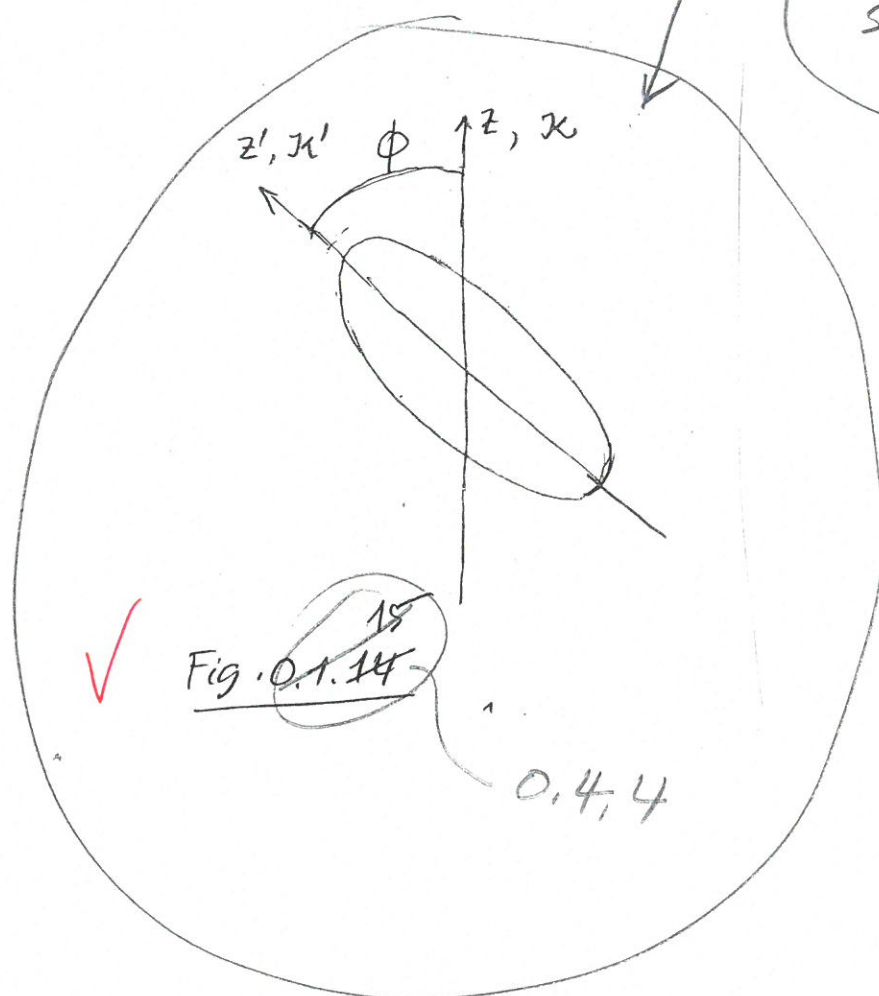


Figure 19. Ground state and excited states in the extreme independent single-particle model and in the pairing-correlated, superfluid model in the case of a system with an odd number of particles. In the first case, the energy of the ground state of the odd system differs from that of the even with one particle fewer by the energy difference $\epsilon_\nu - \epsilon_{\nu'}$, while in the second case by the energy $E_\nu = \sqrt{(\epsilon_\nu - \lambda)^2 + \Delta^2} \approx \Delta$, associated with the fact the odd particle has no partner. Excited states can be obtained in the independent particle case by promoting the odd particle to states above the level ϵ_ν , or by exciting one particle from the state below to the state ϵ_ν or to one above it. To the left only a selected number of these excitations are shown. In the superfluid case excited states can be obtained by breaking of pairs in any orbit. The associated quasiparticle energy is drawn also here by an arrow of which the thin part indicates the contribution of the pairing gap and the thick part indicates the kinetic energy contribution, i.e. the contribution arising from the single-particle motion. Note the very different density of levels emerging from these two pictures, which are shown at the far left of the figure (after Nathan and Nilsson (1965)). Reprinted from *Alpha- Beta- and Gamma-Ray Spectroscopy*, Vol. 1, Nathan, H. and Nilsson, S. G., Editor Siegbahn, H., page 601, Copyright 1965 with permission from Elsevier.

(a) Independent (dashed line) and BCS occupation numbers; (b)

Use Fig. 4.1 p. 78
Brueck + Broglia

also the
same
caption



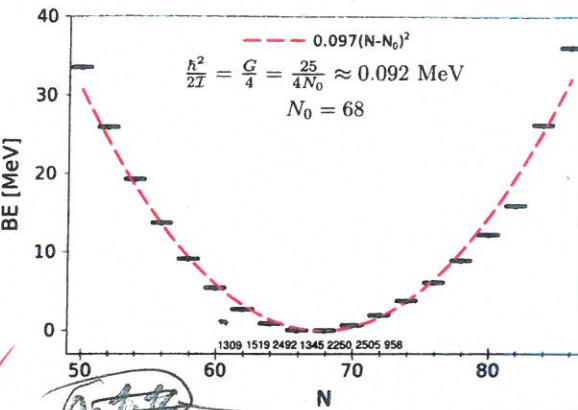


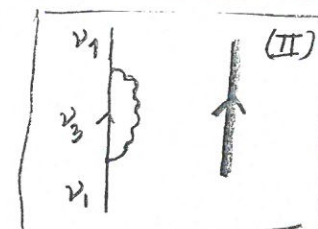
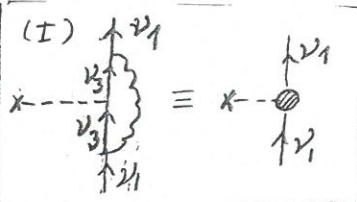
FIG. 9. (Color online) Pairing rotational band along the tin isotopes. The lines represent the energies calculated according to the expression $BE = B(^{50+N}Sn_N) - 8.124N + 46.33$ [10], subtracting the contribution of the single nucleon addition to the nuclear binding energy obtained by a linear fitting of the binding energies of the whole Sn chain. The estimate of $h^2/2I$ was obtained using the single j -shell model (see, e.g., Ref. [10], Appendix II). The numbers given on the abscissa are the absolute value of the experimental $gs \rightarrow gs$ cross section (in units of μb) see Table IV.

After Patel et al (2013)

Sn-isotopes

(see inset (I); the hatched circle in the diagram to the right represents the renormalized density operator; dashed horizontal line starting with a cross and ending at a process displayed to the left.)

VOLUME 59, NUMBER 24



PHYSICAL REVIEW LETTERS

14 DECEMBER 1987

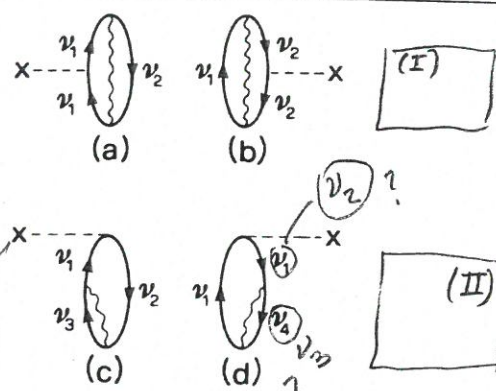


Fig. D.5.1 FIG. 1. Lowest-order corrections in the particle-vibration coupling vertex of the nuclear density due to the presence of zero-point fluctuations associated with density vibrations. An arrowed line pointing upwards denotes a particle, while one pointing downward a hole. A wavy line represents a surface phonon. The density operator is described through a dotted horizontal line starting with a cross. Graphs (a) and (b) are typical examples of density contributions to $\delta\rho$; (c) and (d) are of potential contributions.

After Barranco et al.
(1987)

As expected, fluctuations of the surface remove matter from inside the nucleus and place it on the surface region. The most important contributions arise from low-lying ($T=0, I^\pi=3^-, 5^-$) collective vibrations. From the point of view of the single-particle motion the associated surface fluctuations display very low frequencies and lead to an ensemble of deformed shapes. Nucleons can thus reach into distances from the nuclear center which are considerably larger than the radius R of the static spherical potential. Because the frequencies of the giant resonances ($T=1$ and $T=0, I^\pi=2^+, 3^-, 4^+, 5^-$)

(see inset (I); the dashed horizontal line starting with a cross and ending at a hatched circle in the diagram to the right)

are of similar magnitude to those corresponding to the single-particle motion, the associated surface deformations are averaged out.

On account of the presence of smaller energy denominators, the single-particle renormalization contributions [cf. graphs (c) and (d) of Fig. 1] are much larger than the vertex-type contributions [graphs 1(a) and 1(b)]. In fact $\approx 70\%$ of the total effect arises from the first type of diagrams [cf. Table I and Fig. 2(A)]. Similar results were obtained by Khodel, Platanov, and Saperstein.⁸

Because graphs 1(c) and 1(d) contain scattering vertices, to calculate their contribution one has to go beyond the RPA. This is the reason why in Ref. 4, where only RPA process were considered, $\delta\rho$ was found to be very small.

A rather general argument can be made of why a calculation including only graphs 1(a) and 1(b) is not correct. All four graphs 1(a)-1(d) constitute a set of sum-rule conserving graphs fulfilling the Ward identity.⁹ In particular, in the case of a monopole vibration the cancellation between all four contributions reflects the conservation of the number of particles (cf. Refs. 10-13). The reason why the cancellation between graphs 1(a) and 1(b) is more complete than between 1(c) and 1(d) is to be found in the fact that while the terms of the type 1(a) correspond to one-to-one with those of type 1(b), many more terms occur of the type 1(c), in which a particle is scattered, than of type 1(d), in which a hole is scattered.

In Fig. 2(B) and Table I we compare the results of the present calculations to those of the macroscopic model of Ref. 5, where the problem of the divergence of the zero-point fluctuations of the liquid drop¹⁴ was solved, and where the role played by surface fluctuations in the static nuclear properties was emphasized.

It can be seen that both methods give rather large and

renormalized single-particle state due to the coupling to the vibrations, leading to the self-energy process shown to the left.

TABLE I. Contribution to the mean square radius of ^{40}Ca arising from the zero-point fluctuations associated with surface vibrations whose multipolarity is indicated in the first column. In columns marked (a)+(b) and (c)+(d) under the heading Micr., the summed contributions of the corresponding graphs of Fig. 1 are displayed including the coupling of all the phonons of each multipolarity (100% energy weighted sum rule). The separate contributions for isoscalar and isovector vibrations are shown. Under the heading (a)+(b)+(c)+(d) the total summed contribution of the processes shown in Fig. 1 are displayed. The contribution of the low-lying modes to these values are shown in parentheses. Under the heading Macr., the macroscopic results calculated according to Ref. 5 are displayed. The summed contributions for all types of processes are 0.935 (Micr.) and 0.659 (Macr.).

right, represents the renormalized density operator, resulting from the processes	$\delta\langle r^2 \rangle (\text{fm}^2)$			
	$T=0$		$T=1$	
	Micr.	Macr.	Micr.	Macr.
2^+	0.017	0.028	0.045	0.045
3^-	0.093	0.384	0.477 (0.371)	0.437
4^+	0.037	0.054	0.091	0.110
5^-	0.065	0.169	0.234 (0.123)	0.240 0.014
Total	0.212	0.635	0.847	0.832 0.035

displayed to the left.)

$T=0 \quad 0.847$

$T=1 \quad 0.082$

0.935 fm^2

$$R_0 = 1.2 \times 4^{1/3} \text{ fm} = 4.1 \text{ fm}$$

$$\frac{3}{5} R_0^2 = 10.11 \text{ fm}^2 \cdot \langle r^2 \rangle$$

$$\delta \langle r^2 \rangle \text{ fm}^2 = 0.935$$

$$\frac{\delta \langle r^2 \rangle}{\langle r^2 \rangle}$$

$$\frac{0.935}{10.11} = 0.09$$

$$\frac{0.935}{12.39} = 0.075$$

$$\frac{\delta \langle r^2 \rangle^{1/2}}{\langle r^2 \rangle^{1/2}} = 30\%$$

$$27\%$$

2725

$$\langle r^2 \rangle^{1/2} = 3.52 \text{ fm} \quad (e, e) \text{ Hofstadter}$$

$$\langle r^2 \rangle = 12.39 \text{ fm}^2$$

() collective
0.371 low-lying

$$\frac{0.123}{0.494}$$

$$\frac{0.494}{10.11} = 0.05 \sqrt{5} = 22\%$$

$$\frac{0.494}{0.419} = 0.011 \sqrt{5} = 20$$

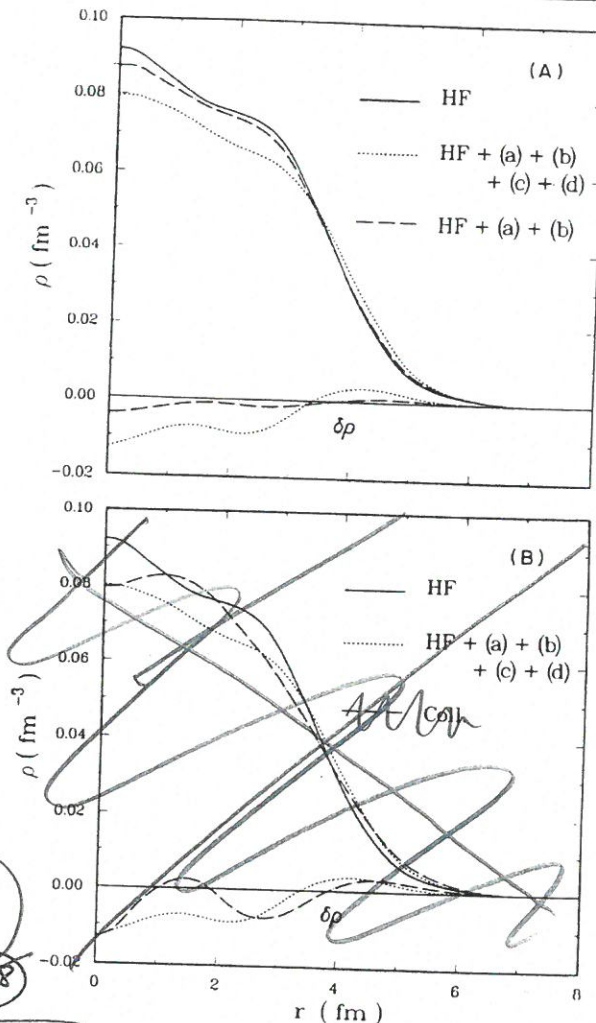


Fig. 2. Modification in the charge density of ^{40}Ca induced by the zero-point fluctuations associated with vibrations of the surface modes. In (A) we show the results of the microscopic calculations presented in this paper. The results labeled HF, HF + (a) + (b), and HF + (a) + (b) + (c) + (d) are the Hartree-Fock density, and that resulting from adding to it the corrections $\delta\rho$ associated with the processes (a) + (b) and (a) + (b) + (c) + (d) displayed in Fig. 1, respectively. In the lower part of the figure the corresponding quantities are displayed. In (B) these results are compared to the macroscopic calculations of Ref. 5.

similar corrections to the mean square radius (cf. the summed contributions at the bottom of Table I). However, the almost perfect agreement between the individual isoscalar contributions of the two models is somewhat misleading. In this connection we point to the negative contributions of the macroscopic model associated with isovector ($T=1$) vibrations. They arise from a (small)

term, linear in the strength of the residual interaction which cancels, to a large extent (exactly in the case of interactions with Serber character, cf. Appendix of Ref. 5, with an analogous but positive linear term present in the isoscalar ($T=0$) channel. This is gratifying, as the lowest-order corrections to the fluctuations of the ground state should be quadratic in the residual interaction. Consequently, it is only the summed [$(T=0) + (T=1)$] contributions which are meaningful in the macroscopic model.

The radial dependence of $\delta\rho$ (cf. Fig. 2) shows maxima and minima out of phase with the Hartree-Fock density displaying, at the nuclear surface, a contribution of the order of 10% of ρ . Fluctuations of the nuclear surface lead to a smoothing of the oscillations of the density and also to an increase in the radius and in the diffusivity of the nucleus. This can be seen in Fig. 2(A), where the microscopic corrections, as well as the Hartree-Fock and the total densities are displayed.

The macroscopic and microscopic results agree well in the surface region [cf. Fig. 2(B)], while the oscillations predicted by the macroscopic model, in the nuclear interior, are more pronounced. In any case, the fact that in the collective approach $\delta\rho \sim \partial^2 \rho / dr^2$ (see Broglia¹⁵) clarifies the phase relation existing between the oscillators in ρ and $\delta\rho$.

The relative change of the mean square radius predicted by the microscopic calculations presented above is $\delta\langle r^2 \rangle / \langle \frac{3}{5} R_0^2 \rangle = 5\%$, in agreement with the results of Ref. 5.

We conclude that the parameters of the effective forces used in Hartree-Fock calculations should not be adjusted to fit the static nuclear properties, but only after the zero-point fluctuations of the surface have been taken into account.

One of us (F.B.) wants to acknowledge economic support from the Spanish Comisión Asesora de Investigación Científica y Técnica. Discussions with G. F. Bertsch and H. Esbensen are gratefully acknowledged.

^(a)Present address: Escuela Superior de Ingenieros Industriales, Avda. Reina Mercedes, Sevilla, Spain.

¹A. Bohr and B. R. Mottelson, *Nuclear Structure* (Benjamin, Reading MA, 1975), Vol. 2.

²P. F. Bortignon, R. A. Broglia, D. R. Bes, and R. Liotta, *Phys. Rep.* **30C**, 305 (1977).

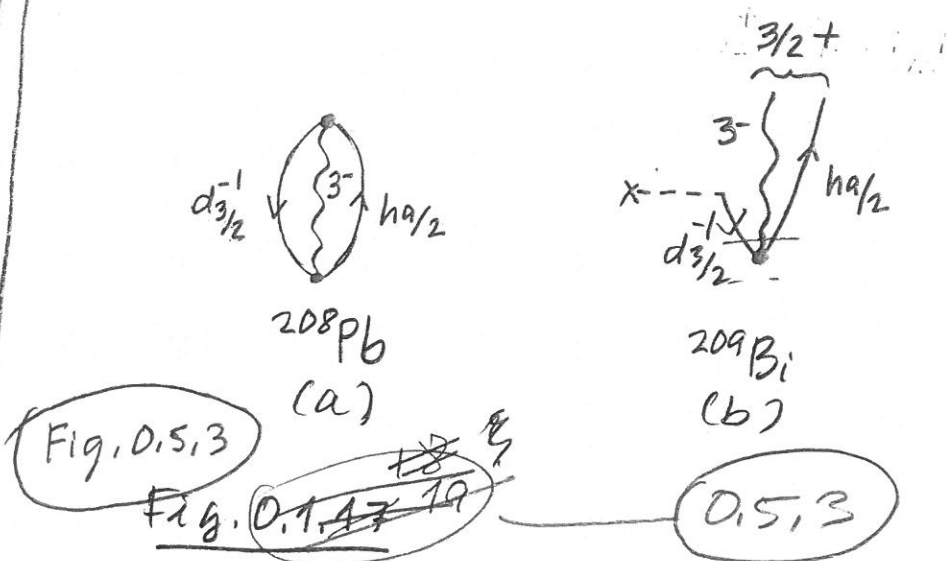
³G. F. Bertsch and S. F. Tsai, *Phys. Rep.* **18C**, 125 (1975).

⁴D. Gogny, in *Nuclear Physics with Electromagnetic Interactions*, edited by H. Arenhövel and D. Drechsel, Lecture Notes in Physics, Vol. 108 (Springer-Verlag, New York, 1979), p. 88.

⁵H. Esbensen and G. F. Bertsch, *Phys. Rev. C* **28**, 355 (1983).

⁶P. G. Reinhard and D. Drechsel, *Z. Phys. A* **290**, 85 (1979).

After Barranco
et al (1987)



(a) zero point fluctuation of the ground state of the double-magic nucleus $^{208}\text{Pb}_{82}^{126}$ associated with the low-lying octupole vibration of this system, observed at and energy of 2.615 MeV and displaying a electromagnetic decay to the ground of 32 Weisskopf units.

(b) ~~Diagrammatic representation of~~

The proton particle-hole component $(h_{9/2}, d_{3/2}^{-1})_3^-$ displayed ~~as the carries the~~ a large amplitude in the octupole vibration wavefunction. (b) Diagram ~~representing~~ the transfer of one proton to $^{209}\text{Bi}_{83}^{126}$, which fills the $d_{3/2}^{-1}$ ~~hole~~ state leading to a $3/2^+$ in $^{209}\text{Bi}_{83}^{126}$, member of the septuplet of states $| (3^- @ h_{9/2}) J^\pi \rangle$ with $J^\pi = 3/2^+, 5/2^+, \dots, 15/2^+$. The horizontal dashed line starting with a cross stand for the stripping process ($^3\text{He}, d$).